instruments

MDPI

Article

Single-Photon Detection Module Based on Large-Area Silicon Photomultipliers for Time-Domain Diffuse Optics

Fabio Acerbi [1,*], Anurag Behera [2], Alberto Dalla Mora [2], Laura Di Sieno [2] and Alberto Gola [1]

[1] Fondazione Bruno Kessler (FBK), Via Sommarive 18, 38123 Trento, Italy; gola@fbk.eu
[2] Dipartimento di Fisica, Politecnico di Milano, Piazza Leonardo da Vinci 32, 20133 Milano, Italy; anurag.behera@polimi.it (A.B.); alberto.dallamora@polimi.it (A.D.M.); laura.disieno@polimi.it (L.D.S.)
* Correspondence: acerbi@fbk.eu

Abstract: Silicon photomultipliers (SiPM) are pixelated single-photon detectors combining high sensitivity, good time resolution and high dynamic range. They are emerging in many fields, such as time-domain diffuse optics (TD-DO). This is a promising technique in neurology, oncology, and quality assessment of food, wood, and pharmaceuticals. SiPMs can have very large areas and can significantly increase the sensitivity of TD-DO in tissue investigation. However, such improvement is currently limited by the high detector noise and the worsening of SiPM single-photon time resolution due to the large parasitic capacitances. To overcome such limitation, in this paper, we present two single-photon detection modules, based on 6 × 6 mm^2 and 10 × 10 mm^2 SiPMs, housed in vacuum-sealed TO packages, cooled to −15 °C and −36 °C, respectively. They integrate front-end amplifiers and temperature controllers, being very useful instruments for TD-DO and other biological and physical applications. The signal extraction from the SiPM was improved. The noise is reduced by more than two orders of magnitude compared to the room temperature level. The full suitability of the proposed detectors for TD-DO measurements is outside the scope of this work, but preliminary tests were performed analyzing the shape and the stability of the Instrument Response Function. The proposed modules are thus fundamental building blocks to push the TD-DO towards deeper investigations inside the body.

Keywords: silicon photomultiplier; diffuse-optics; single-photon; detection module; photodetector

Citation: Acerbi, F.; Behera, A.; Dalla Mora, A.; Di Sieno, L.; Gola, A. Single-Photon Detection Module Based on Large-Area Silicon Photomultipliers for Time-Domain Diffuse Optics. *Instruments* **2021**, *5*, 18. https://doi.org/10.3390/instruments5020018

Academic Editors: Antonio Ereditato and Pasquale Arpaia

Received: 27 April 2021
Accepted: 17 May 2021
Published: 19 May 2021

1. Introduction

Silicon photomultipliers (SiPMs) are highly sensitive, solid-state, versatile and high-performance photodetectors employed in a growing number of applications [1–3]. They are made by arrays of many (hundreds or thousands) single-photon avalanche diodes (SPADs), all connected in parallel to common anode and cathode, but each with its own quenching resistor that quenches the avalanche and restores the operating bias. Each cell (i.e. SPAD + resistor) is sensitive to single photons and provides a defined charge at the SiPM output when an avalanche is triggered. SiPMs have obtained growing attention as an alternative to traditional photomultiplier tubes (PMTs) for detecting low photon fluxes thanks to many advantages typical of solid-state detectors, such as compactness, ruggedness, ease of use, low operational voltage and insensitivity to magnetic fields [1]. Thanks to these advantages, SiPMs are commonly used as light sensors in fast scintillation detectors for X- and gamma-rays, employed in astroparticle physics experiments (e.g., Cherenkov telescope array, CTA), in nuclear medicine (e.g., TOF-PET scanner) and high-energy physics experiments (e.g., DarkSide-20k, GERDA) [4–6]. For example, SiPMs allowed important advancements in positron emission tomography (PET), improving the time resolution of time-of-flight (TOF) PET systems [4].

At Fondazione Bruno Kessler, FBK (Trento, Italy), we have been developing different technologies for SiPMs and SPADs, with different peak sensitivity wavelengths and different characteristics, optimized for diverse applications [7]. SiPMs have been produced

with active area ranging from 1 mm^2 up to 100 mm^2 and with single-cell dimensions (i.e., SPAD) between 10 × 10 μm^2 up to more than 50 × 50 μm^2.

SiPMs are also emerging as very sensitive detectors in many single-photon or few-photon applications, like Cherenkov light detectors [8], light detection and ranging (LIDAR) [9], and biological applications [10,11], thanks to their capability of combining single-photon sensitivity and high dynamic range, their good photon detection efficiency (PDE) and time resolution. In such applications, the parameters of merit and the main constraint are generally different with respect to large-area physics experiments or nuclear imaging systems. For example, applications like Cherenkov detection or LIDAR are based on SiPM pulse detection with a threshold level of a few photons. Other applications, such as in the field of time-domain diffuse optics (TD-DO) like functional near-infrared spectroscopy (fNIRS), are based on single-photon detection, thus using the SiPM as photon-counting detector [11]. In TD-DO, the noise of SiPMs (both the primary noise generation and the correlated noise probabilities, namely afterpulsing and optical crosstalk) is extremely important. It needs to be reduced as much as possible to improve the achievable performances. Moreover, the time resolution at a single-photon level (i.e., single-photon time resolution, SPTR) represents a very important parameter. Particular care must be taken on SiPM optimization and front-end electronics to reduce the noise and extract a prompt signal.

1.1. Time-Domain Diffuse Optics

We focus on using SiPMs in time-domain diffuse-optics. This optical non-invasive technique relies on the injection of fast laser pulses (with a duration in the order of tens of picoseconds) into the medium to be investigated [12,13]. Due to the relatively low absorption of tissue, usually for TD-DO applications, people work in the so-called "therapeutic window" (600–1100 nm). After the propagation of photons in the sample (due to both scattering and absorption events), some are re-emitted from the medium and can be detected at a given distance from the source.

The main advantages of the time-domain technique with respect to the continuous wave (CW) one are: (i) the capability to disentangle the reduced scattering coefficient (μ_s') from the absorption one (μ_a) with a single source-detector pair; (ii) the encoding of the mean penetration depth reached by photons in their arrival time. Indeed, photons that travel for a longer time, thus being later re-emitted, have a higher probability of traveling in deeper regions and investigating their optical properties. Thanks to this higher information content, TD-DO is gaining interest, even though the CW technique typically relies on smaller and less expensive equipment.

In recent years it has become clear that, to approach the physical limits of the technique, one condition to be fulfilled is the increasing of the light harvesting capability of the detector(i.e., detection efficiency, numerical aperture, detector area and fill-factor of the cells over the detector area) [11–14]. In such a scenario, TD-DO systems moved from SPAD to SiPM as detector [11], increasing the light-harvesting thanks to the larger active area and numerical aperture due to the direct contact between the sample and the detector package itself (i.e., avoiding optical fibers in between) [14]. However, two important drawbacks of analog SiPMs are important limitations, especially when moving to an active area larger than few square millimeters: the significant worsening of single-photon time resolution and the increment of dark count rate (DCR). Therefore, currently, only small area SiPMs (1 × 1 mm^2 up to 3 × 3 mm^2) have been used and tested in such applications [15].

1.2. Single-Photon Detection Module for TD-DO

To overcome such limits, thus allowing the use of large-area SiPMs in TD-DO, several improvements are needed, both at system and device levels. In particular: (i) improvement of SiPM layout for better signal extraction and (ii) noise reduction through cooling and through a higher DCR temperature dependence at the SiPM level.

In this paper, we present the design and the characterization of two high-performance, compact, SiPM-based single-photon detection modules designed and assembled in FBK

(Trento, Italy) specifically to be used in TD-DO. In Section 2, we report on the main characteristics of the first module, based on 6 × 6 mm^2 active areas (preliminary described in [16], where can also be found a preliminary performance comparison with other TD-DO instruments) and the second module, based on a 10 × 10 mm^2 area SiPM. In Section 3, we describe the main functional performance of the two modules, like noise, detection efficiency, time resolution. Finally, we show a preliminary evaluation of the suitability of the two modules in TD-DO, the instrument response function (IRF) and its stability over time when coupled to existing TD-DO systems.

2. SiPM Modules Description

The two SiPM-based single-photon detection modules presented in this paper use TO packages with integrated Peltier thermoelectric coolers (TEC) and a negative temperature coefficient (NTC) resistor for temperature regulation. Both the modules include a front-end board for signal amplification and a TEC driving board for temperature regulation. Particular attention was given to reduce any possible electrical interference of the TEC or NTC on the SiPM signal, avoiding high-frequency switching (e.g., proper grounding and shielding, use of linear or on/off controllers).

The first module, shown in Figure 1a, is compact, 5 × 5 × 4 cm^3, and is made by a front aluminum heat sink and a back 3D printed enclosure. The aluminum block contains threaded holes both for fixing the PCB inside and for connecting to optical components outside. The module is based on a large area SiPM of 6 × 6 mm^2 nominal active areas, which is made by 4 different SiPM chips (each one with a dimension of about 3 × 3 mm^2, with 35 µm cell pitch) placed side-by-side, all electrically connected in parallel with common back contact. These SiPMs are designed and fabricated at FBK (Trento, Italy). The cell fill factor for the single SiPM is > 80%. Considering the chip borders, the overall effective active area of the whole sensor is about 32.1 mm^2. The SiPMs are based on the vacuum ultraviolet, high-density (VUV-HD) low-field technology. Despite the peak PDE not well matched to the wavelength range of the TD-DO application, this was chosen because of the low primary noise (DCR) and its high variation with temperature and the lower correlated noise, particularly afterpulsing [17].

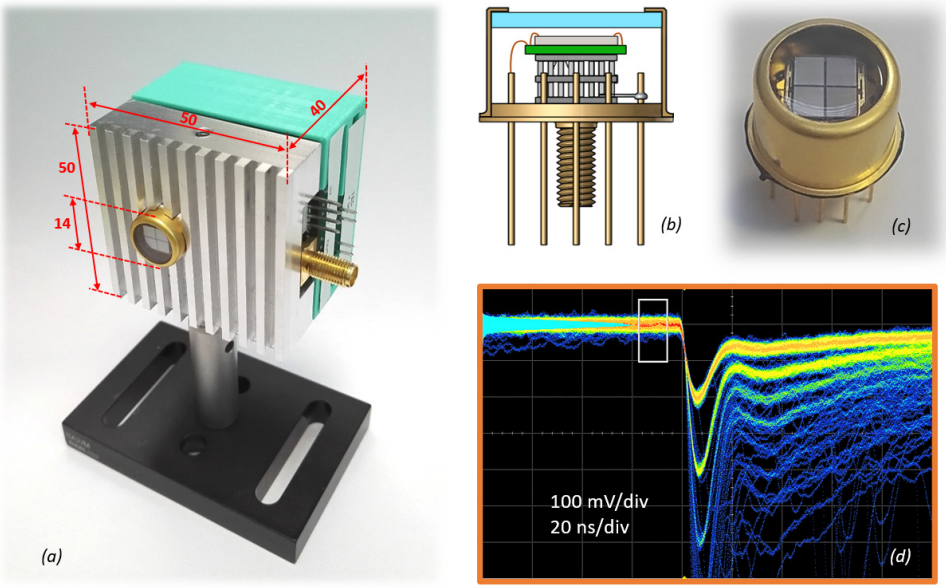

Figure 1. Picture and dimensions of the 6 × 6 mm^2-SiPM detection module, showing the custom heat sink and the connection on the side. Control and front-end circuitry is included (**a**). Schematic representation of internal structure (**b**) and picture (**c**) of the TO8 package containing TEC, temperature sensor, and the SiPM on a 0.5 mm thick PCB. Oscilloscope persistence trace of the output signals at 5.9 V of excess bias with the histogram of the baseline (left side), evaluated within the white box (**d**).

The SiPMs are cooled to about −15 °C inside a vacuum-sealed TO8 package (thus external glass window and the package surface are at room temperature). In this package, there is a 2-stage TEC with 6 × 6 mm^2 areas, with glued NTC on the top stage. On top of this, there is a small (0.5 mm thick) and high-density (4 layers) PCB with buried holes to have good heat conduction, but without electrical conduction up to the top layer, as shown in Figure 1b,c. Indeed, on the top layer, the SiPM chips are glued with electrically conductive glue, being the backside of the silicon chip the cathode of the SiPMs. This must be electrically isolated from the TEC. Moreover, to further reduce any possible electrical interference on the SiPM signal, the internal layers of the PCB were electrically connected to the ground through a wire bond to a pin of the TO package.

An improved signal extraction is also very important to obtain a good single-photon time resolution. This has been accomplished thanks to the improvement of (i) interconnections between the SiPM and the front-end, with multi-wire bonding, (ii) layout of the SiPM metal layer, to amplify the fast-peak component of the signal, as suggested in [18], and (iii) front-end board, with a higher trans-impedance gain of ~10000 V/A. The results are reported in Figure 1d, showing the persistence trace acquired by an oscilloscope with SiPM at 5.9 V of excess bias (i.e., the difference between bias and breakdown voltage). The signal-to-noise ratio, defined as amplitude over the standard deviation of the electronic noise, is about 20. The total power consumption of this module is around 0.9 W.

The schematic representation of the system is shown in Figure 2. Note that the amplifier schematic is the same for the 10 × 10 mm^2 SiPM modules. The SiPM has a breakdown voltage of 33 V at room temperature, reducing to 31.6 V when cooled at −15 °C. Two groups of SiPM (i.e., left ones and right ones, as represented in Figure 1c) are connected separately to the amplifier and then summed at the virtual ground node. Figure 2 also shows the equivalent electrical circuit of the SiPM. Increasing the area increases the number of passive cells and the grid capacitance (Cg), which accounts for the capacitance of all the metal lines on top of the device. Both these effects create a low pass filtering on the signal of the triggered cell (in the case of one-photon absorption), lowering its rising edge slope and amplitude, as reported in [19].

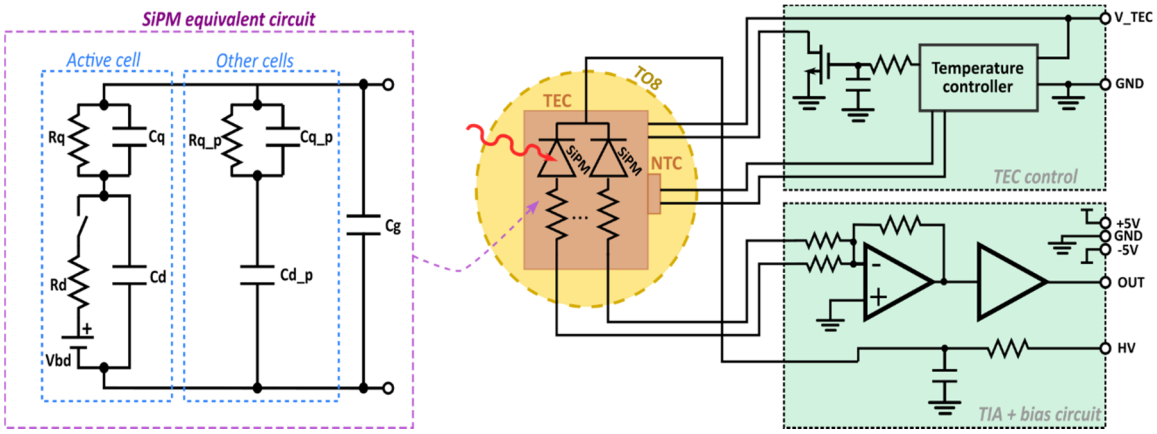

Figure 2. Schematic of the control circuit and front-end circuit included in the 6 × 6 mm^2-SiPM module. The SiPMs, TEC and NTC are included in the TO8 package. The SiPM equivalent electrical circuit is also represented in the case of 1 triggered cell. Rq is the quenching resistor, with its parasitic capacitance (Cq), Cd is the diode capacitance, Rq_p, Cq_p, Cd_p are the same as non-triggered cells, Cg is the capacitance of the top metal grid (see [3]).

The second module is shown in Figure 3. The dimensions are 6.0 × 7.3 × 5.8 cm^3, including the backside fan, resulting in bigger than the previous module, mainly because of the higher heat to be dissipated. It is still made with a metal heat sink on the front and a 3D printed backside enclosure. It is based on a 10 × 10 mm^2 SiPM, specifically designed and fabricated at FBK. This is made in a modified NIR-HD technology [7,20], with a 50 µm cell pitch and an adapted layout to improve the signal extraction for the single

cells. The SiPM, despite being a single silicon chip, is internally divided into 6 sub-SiPMs (about 4.88 × 3.25 mm^2 area), externally connected together in 2 groups, then the signals are merged at the front-end, as schematized in Figure 2. The package is a TO822 can, with a custom-made cap with an optical window made by 2 pieces of borosilicate silicon dioxide glass, 0.5 mm thick, glued together and then glued to the aluminum frame as shown in Figure 3b. The total number of bonding wires from the SiPM chip is 18, i.e., 9 per each side. There is still the connection of the internal PCB's layers to the ground to reduce the TEC and the NTC interference on the SiPM signal, as represented in Figure 3c. The typical output signal is represented in Figure 3d, being approximatively 200 mV, with a rising edge of 4.2 ns (10–90%), an FWHM of 11.7 ns and a tail with 100 ns time constant.

The temperature controller is a liner stage, based on the WHY5640 [21] module, with a custom small-dimension heat sink. The TEC inside the package is a 2 stage 11.4 × 11.4 mm^2 Peltier. The SiPM is cooled down to about −36 ± 1.5 °C. Such low temperature is necessary to reach a primary dark count rate of the SiPM of about 1 Mcps (counts per second), considered as the maximum acceptable threshold for the TD-DO application. This estimation has been done for a detection module with a different IRF. It derives from a complex interplay between instrumental, optical and geometrical parameters, as shown in [22]. However, the effect of the noise floor in the achievable depth sensitivity does not change dramatically even using an IRF with larger FWHM (e.g., 560 ps as in [15]).

The total power dissipation of the TEC is about 6.5 W. To cool down the front heat-sink, and the TEC controller one, a 60 × 60 mm^2 fan was placed on the back of the module. The front-end, the temperature controller and the ancillary electronics are supplied with ±5 V and +10 V biases.

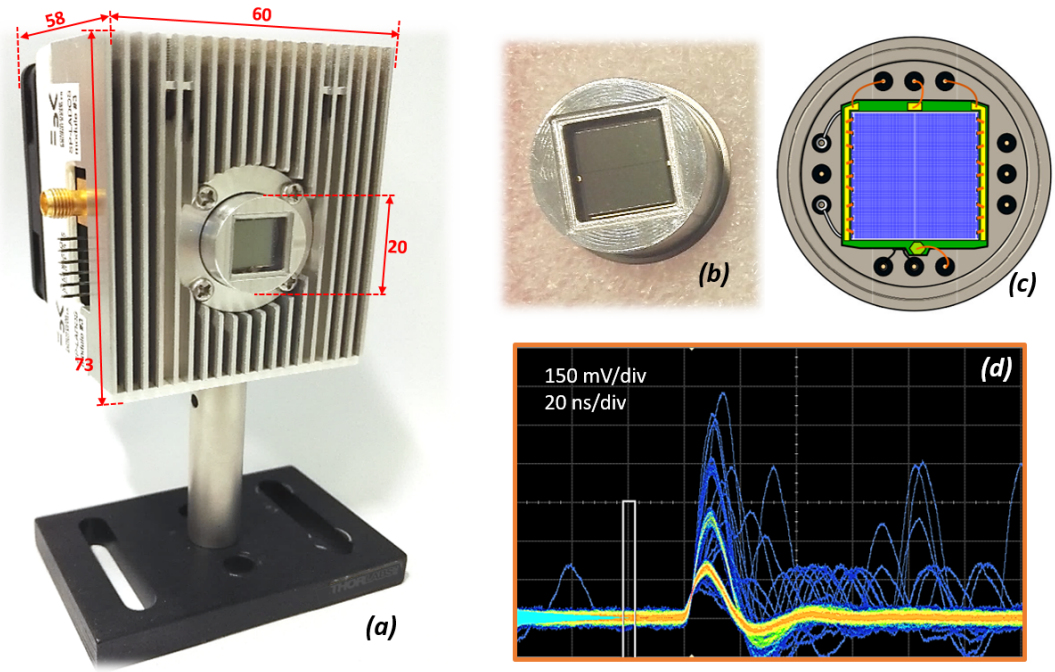

Figure 3. Picture and dimensions of the 10 × 10 mm^2-SiPM detection module, made of an aluminum heat sink, 3D printed enclosure with DC fan on the back (**a**). Picture (**b**) and schematic representation (**c**) of the TO822 package with custom large-optical windows cap. Oscilloscope persistence trace of the output signals at 4.9 V of excess bias, with a histogram of the baseline (left side), evaluated within the white box (**d**).

3. Measurement Results

We tested the main functional performance of both the single-photon detection modules. The noise and the signal amplitude have been tested with the method described in [3,7]. Specifically, we collected 1 ms long frames of output signals, applied differential leading-edge discrimination filters (DLED) with undershoot compensation to reduce the effect of the signal pile-up. Then we identified the amplitude and the inter-arrival time of all the pulses using a discrimination threshold equal to half the single-cell signal amplitude. Then, building a scatter plot and histograms of amplitudes and inter-times, we could distinguish the primary thermal-generated dark counts, the afterpulsing and the optical crosstalk pulses.

3.1. Performance of 6 × 6 mm² SiPM Modules

The measurement results on the 6 × 6 mm^2-SiPM module are shown in Figure 4. The primary noise (dark count rate, DCR), i.e., the thermal, field-assisted generation of electron–hole pairs, is 325 kcps at 5 V of excess bias (i.e., ~8.8 kcps per 1 mm^2 of active area). It increases linearly with the bias, whereas the total DCR (including also delayed correlated noise) is 360 kcps. This value is obtained from the 6 × 6 mm^2 SiPM cooled at −15 °C. The reduction of DCR with respect to room temperature is greater than 15 times, thanks to the increased temperature dependence of the DCR in the specific SiPM technology employed. The micro-cell gain, measured as the total charge provided from the single-cell pulse, is ~2.2 × 10^6 at 5 V of excess bias, while the single-cell pulse amplitude is about 177 mV (Figure 4b).

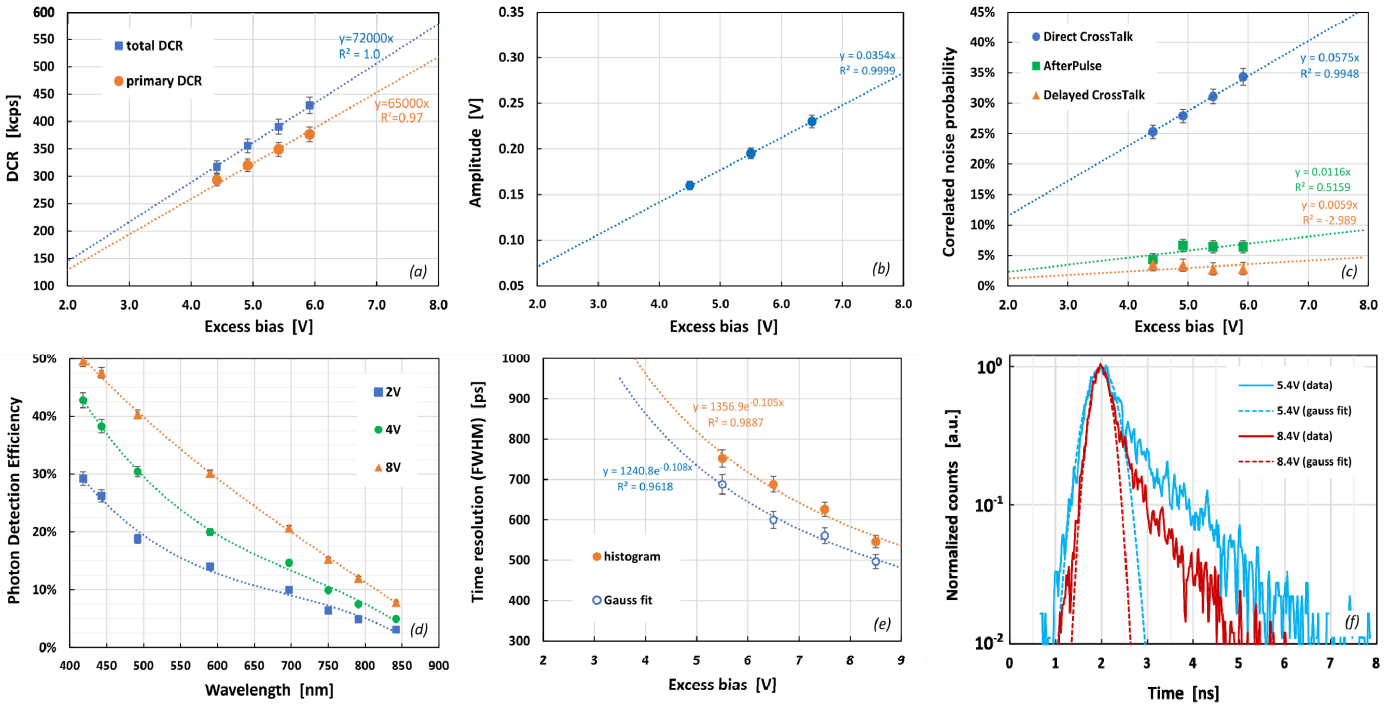

Figure 4. Measured performance of 6 × 6 mm^2-SiPM modules, with SiPM, cooled at −15 °C. Primary and total dark count rate, DCR (**a**), single-cell signal amplitude at the output of the module (**b**), correlated noise probabilities (**c**), the photon detection efficiency of the SiPMs, including FF (**d**). Single-photon time resolution, measured as in [19] with 830 nm laser (FWHM of timing histogram and Gaussian fit) (**e**), with two examples of timing histograms (**f**).

The correlated noise considers all the noisy pulses generated because of a primary one (either photon or thermal generated). We distinguish afterpulsing, primary (or prompt) optical crosstalk and the delayed optical crosstalk probability [7], shown in Figure 4c. The direct crosstalk is 28.7%, at 5 V of excess bias, while the afterpulsing and delayed crosstalk (which represents the so-called "delayed correlated noise") is ~5.8% and ~3%, respectively. The delayed correlated noise increases when decreasing the temperatures because of both the longer traps release time and the higher carrier lifetime. Thus these probabilities are higher than at room temperature, as reported in [17]. We also measured the PDE (Figure 4d), using pulsed LED illumination, with the method and the setup reported in [23]. We used several LED wavelengths (indicated by the markers in the plot), and the curve was fitted with polynomial curves. At 700 nm, the PDE is ~14% with 4 V and increases at 20% with 8 V. At 850 nm, it is ~5% with 4 V of excess bias, whereas it increases to 7.5% with 8 V.

Finally, we measured the single-photon time resolution (SPTR) using an 830 nm pulsed laser, attenuated and shined towards the active area of the SiPM. When measuring the SPTR, using the technique and the setup described in [19], we must consider only the event when just one micro-cell of the SiPM is triggered by the laser pulse. Otherwise, the different signal amplitude and the different statistics in avalanche triggering would affect the result. This is done with proper event selection based on pulse amplitude, as reported in [19]. The obtained SPTR expressed as full-width at half maximum (FWHM) is shown in Figure 4e, which includes the time resolution FWHM, considering both the whole histogram and the FWHM of the Gaussian fit on the first part of the histogram. A couple of examples of timing histogram (corresponding to different excess biases) are reported in Figure 4f. It can be seen that the timing histogram shape is composed of a main Gaussian peak and a tail. The former is due to avalanche buildup statistics and baseline fluctuation (see [18]). It generally worsens when using large-area SiPMs, because of the low-pass filtering effect on the signal slope and the higher noise of the detector. The latter, i.e., the tail, is due to photon absorbed in neutral regions in the device, then diffusing slowly towards the active area and then triggering an avalanche pulse with a certain delay. The latter component is particularly detrimental for TD-DO [22]. It should be minimized, for example, by modifying the SPAD structure or by using different silicon starting material (e.g., using inverted junction in the substrate like in [24]). Overall, the SPTR of the 6×6 mm^2 SiPM modules is ~600 ps (with 7.7 V excess bias), with a tail time constant of about 1 ns.

3.2. Performance of 10 × 10 mm^2 SiPM Module

We tested the performance of the larger-area SiPM module as well, with the same procedures. The measured performances are shown in Figure 5. As described earlier, this module is not just a bigger version of the previous one. Indeed, it employs a SiPM made with a different technology, specifically conceived to have higher sensitivity in the red and NIR wavelength regions. In particular, a p-type substrate (instead of n-type) with an n-on-p junction has been used. As a result, the polarity of the bias is inverted, and the polarity of the output signal as well. The measured DCR is shown in Figure 5a. Thanks to the stronger cooling (-36 °C), the primary noise is ~850 kcps (i.e., ~8.5 kcps per 1 mm^2 of active area), whereas the total DCR 900 kcps at 5 V of excess bias. The signal amplitude is still 186 mV, at 5 V, despite the bigger dimensions, which implies a bigger filtering effect. This was possible thanks to the improved layout and the larger micro-cell in the SiPM. The correlated noise probability is shown in Figure 5c. The direct crosstalk probability is 22.4% at 5 V, while both the afterpulsing and the delayed crosstalk are in the order of 2%. Figure 5d shows the photodetection efficiency as a function of the wavelength. It can be seen that the peak has now moved towards the orange-wavelength part of the spectrum. The PDE is 28.6% at 600 nm with 4 V excess bias and 38% with 8 V. At 700 nm, it is 35.5% at 8 V, whereas, at the same bias, it is still higher than 11% at 900 nm.

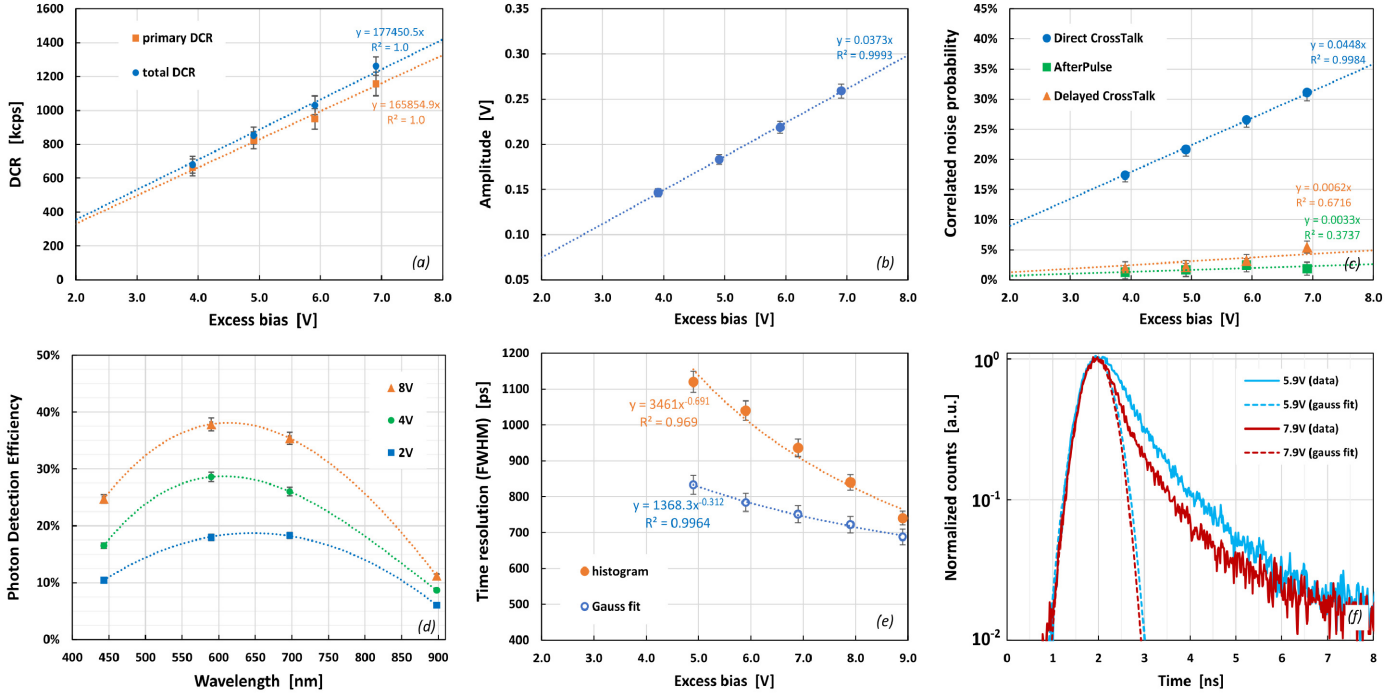

Figure 5. Measured performance of 10 × 10 mm^2-SiPM modules, with SiPM, cooled at −36 °C. Primary and total dark count rate, DCR (**a**), single-cell signal amplitude at the output of the module (**b**), correlated noise probabilities (**c**), photon detection efficiency, including FF (**d**). Single-photon time resolution, measured as in [19] with 830 nm laser (FWHM of timing histogram and Gaussian fit) (**e**), with two examples of timing histograms (**f**).

As for the previous module, we measured the single-photon time resolution of the 10 × 10 mm^2 SiPM modules, using an attenuated 830 nm pulsed laser, shined on the large-area SiPM through a glass diffuser to have uniform light illumination. The results are reported in Figure 5e, including the time resolution FWHM, considering both the whole histogram and the FWHM of the Gaussian fit on the first part of the histogram. A couple of examples of timing histograms are reported in Figure 5f. It can be seen that the main peak is wider than for the previous SiPM module. This is mainly due to the higher noise contribution [18] with such a large area detector. In contrast, the tail after the peak seems to be the superposition of different time constants. Overall, the tail-part amplitude is higher (more important) than in the previous SiPM module, mainly because in such NIR-HD technology, the carrier's photo-generated in-depth in the epitaxial layer triggers the avalanche using electrons, thus having a higher triggering probability [7]. This is the reason for the higher PDE, but it resulted in a larger tail in the timing histogram. In this case, a tradeoff is needed in the detection system design, between the PDE, which is important in increasing the light-harvesting capabilities, and the shape of the timing histogram, which is linked to the ability to distinguish properties of the tissue in TD-DO [11,20].

3.3. Preliminary Time-Domain Diffuse Optics Tests

A full evaluation of the modules' performances in TD-DO requires requires the application of several tests aiming to a full evaluation of basic hardware performances, capability to recognize absolute homogeneous/heterogeneous optical properties and the capability to detect, localize and quantify optical perturbation. This will result in a comprehensive study linked to the particular system, and it is outside the scope of this work. However, to preliminary evaluate the suitability of the proposed SiPM modules for time-domain applications, we evaluate their IRF and its stability, as dictated by the basic instrumental performance (BIP) protocol [25], combining them to an existing state-of-the-art TD-DO system in Politecnico di Milano (Milano, Italy). The IRF estimates the time resolution of the detector when used in the TD-DO setup, and its shape is crucial in the retrieval of

optical properties [22]. Its stability (evaluated in terms of FWHM, barycenter and temporal position) is fundamental to assess the capability of a time-domain instrument to measure small changes in photon flight time (e.g., physiological changes induced by functional stimulation of the brain). These characterizations are interesting as they can, for instance, already permit to estimate in silico the performances of different systems using this detector technology [22].

The IRF has been measured with a setup based on a SuperK EXTREME (NKT Photonics, Denmark) supercontinuum laser operating at a repetition rate of 40 MHz. Output wavelength has been selected with a controlled rotating prism. The output light intensity was regulated using a circular variable neutral density filter to have a photon count rate of about 1.5 Mcps at the detector. The attenuated light, after passing a thin layer of Teflon to ensure the mix of all the propagation modes of the fiber and the illumination of the whole active area with Lambertian distribution (i.e., the reference condition for TD-DO), was sent on the active detector area. The output signal of the SiPM module was sent to the time-correlated single-photon counting (TCSPC) board (SPC-130, Becker & Hickl GmbH, Berlin, Germany) as a start signal. At the same time, the stop one, synchronous with laser pulses, was provided by the laser unit. A picture of the setup is reported in Figure 6. For each wavelength, five repetitions of 1 s were recorded. All the repetitions were summed up to improve the signal-to-noise ratio (e.g., reducing the Poisson noise relative contribution). As a last step for the data analysis, the background (computed as the mean value of counts in the region before the peak) was subtracted.

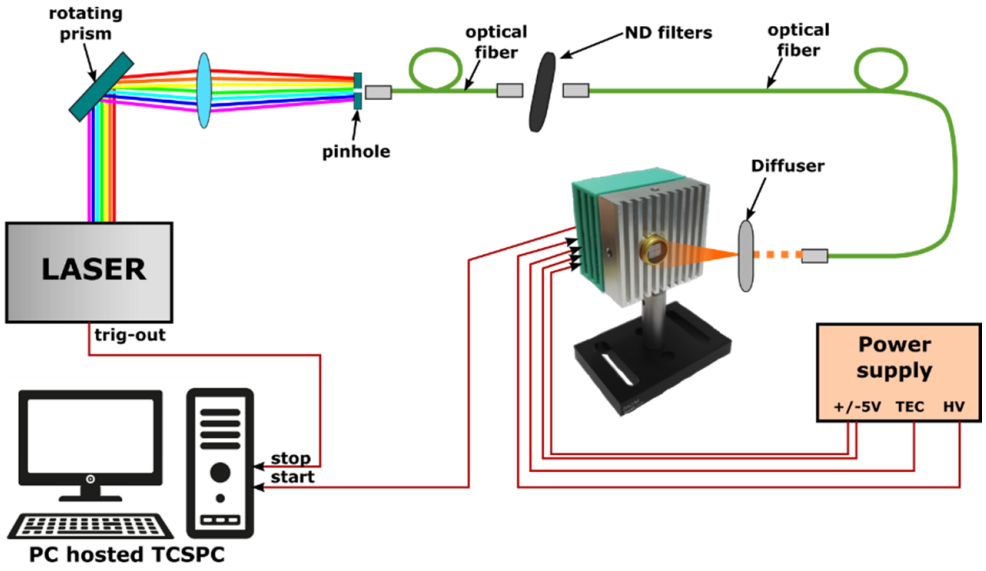

Figure 6. Setup used for the preliminary evaluation of the SiPM modules in time-domain diffuse optics.

The shape of the IRFs of the two modules is reported in Figure 6a,d (for 6×6 mm^2 and 10×10 mm^2 SiPM, respectively). It is worth noting that the TCSPC board uses a constant fraction discriminator and does not discriminate the avalanche pulses amplitude. This is not exactly the same as the SPTR measurements, likely because of the different setup and the different input detection methods. In both SPTR and IRF measurements, the average number of photons detected per laser pulse is much lower than 1, typically <0.05 to avoid distortion of timing histogram [26], thus practically statistically excluding the possibility to have the simultaneous detection of two or more photons. However, in SPTR measurement, only 1-photon amplitude events are selected (e.g., also discarding the cases with 1 absorbed photon followed by optical crosstalk events between SiPM cells). Instead, for measurements reported in this section, all the avalanche pulses are recorded to avoid losing photons coming from the tissue every time an optical crosstalk event is generated. As the avalanche pulse amplitude depends on the presence of crosstalk,

this effect could be, in principle, expected to distort the IRF shape. However, crosstalk effects can be profitably mitigated thanks to the constant-fraction discriminator on the input channels of the TCSPC board, which are specifically designed to strongly reduce the dependence of TCSPC histograms on amplitude changes of the electrical signals. As a matter of fact, despite being present in all SiPMs, optical crosstalk has not limited the growing adoption of SiPM in TD-DO [11].

The IRFs are shown for different wavelengths, between 600 nm and 1100 nm. The obtained time resolution FWHM are reported in Figure 7b,e, between 550 ps and 720 ps for the first module and between 725 ps and about 1 ns for the second module, depending on the wavelength. The difference between the two is likely due to the wider SPTR of the second module. In contrast, the worsening when increasing the wavelength can be ascribed to the higher percentage of light absorbed in-depth in the neutral regions, thus giving a wider spread in avalanche buildup times and a higher tail amplitude relative tothe main peak.

As dictated by the BIP protocol, we also measured the stability of the IRF, i.e., the stability over time of the IRF FWHM, barycenter and the total count rate of the detector. For both modules, we considered a 30 min warm-up time. Figure 7c shows the variation of the considered parameters (IRF FWHM, counts and barycenter) with respect to the average value. For the 6 × 6 mm^2 SiPM modules, the total count rate and the IRF barycenter are very stable over 10 h of operation. In particular, after 2 h, a variation of less than ±0.5% (i.e., ±4 kcps) and ±0.2% (i.e., ±1.7 ps) are present, respectively. The IRF FWHM has a maximum variation of less than ±1.5% (i.e., ±9 ps). Figure 7f shows the stability over 6.5 h of the 10 × 10 mm^2 SiPM modules. This is very stable as well, especially after 1 h. The total count variation is within ±0.3% (i.e., 27 kcps). In contrast, the IRF barycenter and FWHM show a variation of less than 0.6% (i.e., ±24 ps) and 1–1.5% (i.e., ±10 ps), respectively. Overall, the temporal stability is appropriate for the application is in line with state-of-the-art TD-DO systems [27,28].

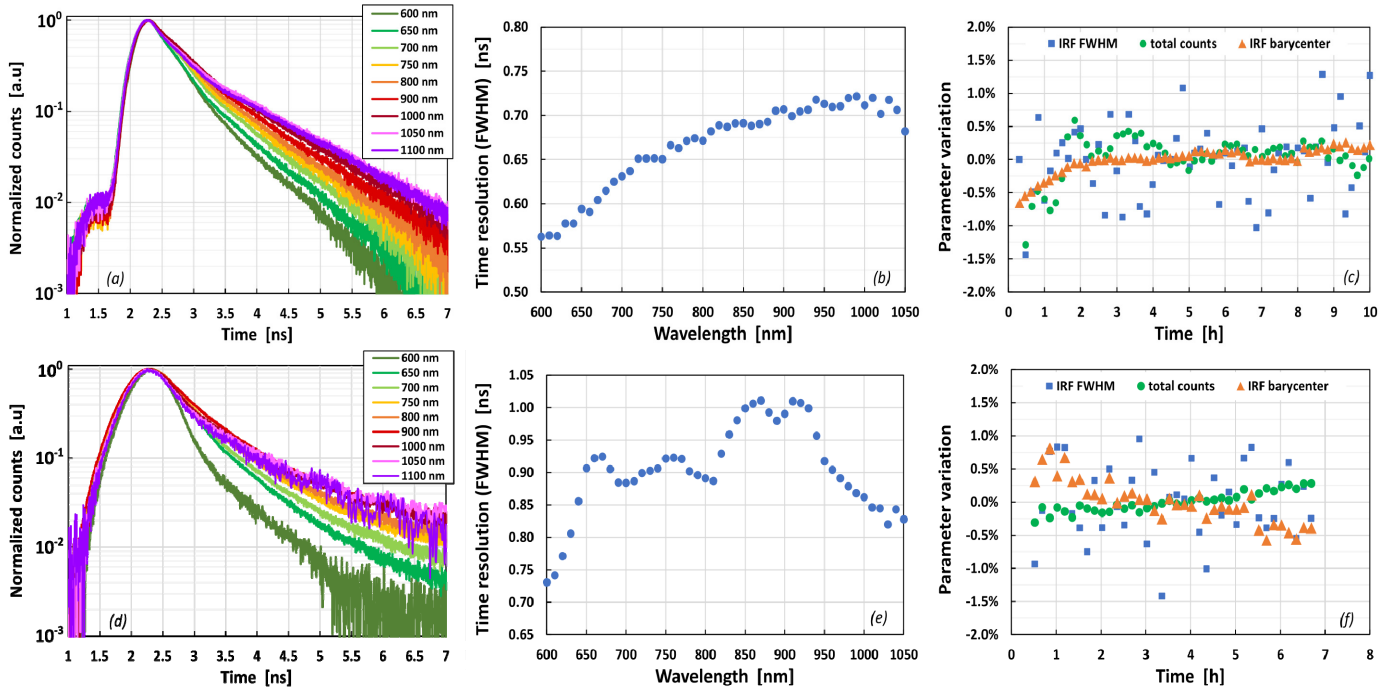

Figure 7. Measured instrument response function for TD-DO, using a supercontinuum laser illuminating the 6 × 6 mm^2 SiPM modules (**a**) and the 10 × 10 mm^2 SiPM modules (**d**). The relative histogram width, FWHM, for the different wavelengths in the plots (**b**,**e**), respectively. The IRF stability (with 670 nm laser) of FWHM, barycenter and total counts over hours are reported in the plot (**c**,**f**) again for the former and latter modules, respectively.

4. Conclusions

We described the main characteristics of two different large-area (i.e., 6 × 6 mm^2) and very-large area (i.e., 10 × 10 mm^2) SiPM-based single-photon detection modules. These have been developed within ATTRACT project SP-LADOS [16] to be used in time-domain diffuse-optics applications. In particular, these large-area detectors can have important advantages in such applications, significantly increasing the sensitivity with respect to the state-of-the-art. This higher sensitivity, combined with a moderate noise rate and a good time resolution, can significantly improve the performance of TD-DO measurements and could allow in the near future to investigate deeper tissues, theoretically enabling to probe organs in-depth or even the chest in transmission geometry.

The 6 × 6 mm^2 SiPM has passive cooling and low-power consumption. It is based on a SiPM technology more sensitive in the blue wavelength region. Still, it can also work in other regions of the visible and NIR spectrum. It showed a noise level in the order of 300 kcps (i.e., around 9 kcps/mm^2) when cooled by the internal Peltier module, and a time resolution in the order of 600 ps FWHM. The larger (10 × 10 mm^2) SiPM module is based on a NIR-HD (modified) technology. It is based on a similar design concept. It showed a detection efficiency peaked in the green wavelength region, reaching almost 40% and still higher than 11% at 900 nm. The noise level is around 800 kpcs (i.e., around 8 kcps/mm^2) when cooled. The single-photon time resolution is in the order of 900 ps.

The suitability for TD-DO measurements of both these modules was tested acquiring the IRF (when coupled to an existing TD-DO system). The recorded FWHM at 700 nm is around 640 ps for the first module and about 900 ps for the second module. The stability in performance over several hours of operation was also evaluated. It is good and in line with the state-of-the-art system, with maximum variations in the order of ±1%.

These good performances (i.e., DCR < 1 Mcps, time resolution of hundreds of picoseconds, and active areas of 6 × 6 mm^2 or 10 × 10 mm^2) make these detection modules interesting instruments for TD-DO and other photon-counting-based applications where high-sensitivity, a large detection area and a high dynamic range (in terms of minimum and maximum counting rate, as well as photon number resolution), are important features. Furthermore, future improvements in performance could be obtained by investing the possibility to create large-area tiles of SiPMs, following the approaches described in this work.

Author Contributions: Conceptualization, F.A., L.D.S., A.D.M.; methodology, F.A., L.D.S., A.B., A.D.M., A.G.; writing—original draft preparation, F.A.; writing—review and editing, F.A., L.D.S., A.D.M., A.B.; project administration, F.A.; funding acquisition, F.A., L.D.S. All authors have read and agreed to the published version of the manuscript.

Funding: This research has received funding from the ATTRACT project funded by the EU under Grant Agreement 777222 and from European Commission under the H2020 framework with the BITMAP project 675332.

Data Availability Statement: Data sharing not applicable.

Conflicts of Interest: The authors declare no conflict of interest.

References

1. Renker, D. Geiger-mode avalanche photodiodes, history, properties and problems. *Nucl. Instrum. Methods Phys. Res. Sect. A* **2006**, *567*, 48–56. [CrossRef]
2. Gundacker, S.; Heering, A. The silicon photomultiplier: Fundamentals and applications of a modern solid-state photon detector. *Phys. Med. Biol.* **2020**, *65*, 17TR01. [CrossRef]
3. Acerbi, F.; Gundacker, S. Understanding and simulating SiPMs. *Nucl. Instrum. Methods Phys. Res. Sect. A* **2019**, *926*, 16–35. [CrossRef]
4. Moses, W.W. Recent advances and future advances in time-of-flight PET. *Nucl. Instrum. Methods Phys. Res. Sect. A* **2007**, *580*, 919–924. [CrossRef]
5. Bisogni, M.G.; Del Guerra, A.; Belcari, N. Medical applications of silicon photomultipliers. *Nucl. Instrum. Methods Phys. Res. Sect. A* **2019**, *926*, 118–128. [CrossRef]

6. Simon, F. Silicon photomultipliers in particle and nuclear physics. *Nucl. Instrum. Methods Phys. Res. Sect. A* **2019**, *926*, 85–100. [CrossRef]
7. Acerbi, F.; Paternoster, G.; Capasso, M.; Marcante, M.; Mazzi, A.; Regazzoni, V.; Zorzi, N.; Gola, A. Silicon Photomultipliers: Technology Optimizations for Ultraviolet, Visible and Near-Infrared Range. *Instruments* **2019**, *3*, 15. [CrossRef]
8. Korpar, S.; Dolenec, R.; Križan, P.; Pestotnik, R.; Stanovnik, A. Study of TOF PET using Cherenkov light. *Nucl. Instrum. Methods Phys. Res. Sect. A* **2011**, *654*, 532–538. [CrossRef]
9. Son, K.T.; Lee, C.C. Multiple-Target Laser Range finding Receiver Using a Silicon Photomultiplier Array. *IEEE Trans. Instrum. Meas.* **2010**, *59*, 3005–3011. [CrossRef]
10. Zimmermann, R.; Braun, F.; Achtnich, T.; Lambercy, O.; Gassert, R.; Wolf, M. Silicon photomultipliers for improved detection of low light levels in miniature near-infrared spectroscopy instruments. *Biomed. Opt. Express* **2013**, *4*, 659–666. [CrossRef] [PubMed]
11. Dalla Mora, A.; Di Sieno, L.; Behera, A.; Taroni, P.; Contini, D.; Torricelli, A.; Pifferi, A. The SiPM revolution in time-domain diffuse optics. *Nucl. Instrum. Methods Phys. Res. Sect. A* **2020**, *978*, 164411. [CrossRef]
12. Yamada, Y.; Suzuki, H.; Yamashita, Y. Time-Domain Near-Infrared Spectroscopy and Imaging: A Review. *Appl. Sci.* **2019**, *9*, 1127. [CrossRef]
13. Jacques, S.L. Time-resolved reflectance spectroscopy in turbid tissues. *IEEE Trans. Biomed. Eng.* **1989**, *36*, 1155–1161. [CrossRef]
14. Re, R.; Martinenghi, E.; Mora, A.D.; Contini, D.; Pifferi, A.; Torricelli, A. Probe-hosted silicon photomultipliers for time-domain functional near-infrared spectroscopy: Phantom andin vivotests. *Neurophotonics* **2016**, *3*, 045004. [CrossRef] [PubMed]
15. Di Sieno, L.; Behera, A.; Rohilla, S.; Ferocino, E.; Contini, D.; Torricelli, A.; Krämer, B.; Koberling, F.; Pifferi, A.; Dalla Mora, A.; et al. Probe-hosted large area silicon photomultiplierand high-throughput timing electronics for enhanced performance time-domain functional near-infrared spectroscopy. *Biomed. Opt. Express* **2020**, *11*, 6389–6412. [CrossRef] [PubMed]
16. ATTRACT Project. Innovative Single-Photon Large-Area Optical Probe for Diffuse Optical Spectroscopy. Available online: https://attract-eu.com/showroom/project/innovative-single-photon-large-area-optical-probe-for-diffuse-optical-spectroscopy-sp-lados (accessed on 16 April 2021).
17. Capasso, M.; Acerbi, F.; Borghi, G.; Ficorella, A.; Furlan, N.; Mazzi, A.; Merzi, S.; Mozharov, V.; Regazzoni, V.; Zorzi, N.; et al. FBK VUV-sensitive Silicon Photomultipliers for cryogenic temperatures. *Nucl. Instrum. Methods Phys. Res. Sect. A* **2020**, *982*, 164478. [CrossRef]
18. Acerbi, F.; Ferri, A.; Gola, A.; Zorzi, N.; Piemonte, C. Analysis of single-photon time resolution of FBK silicon photomultipliers. *Nucl. Instrum. Methods Phys. Res. Sect. A* **2015**, *787*, 34–37. [CrossRef]
19. Acerbi, F.; Ferri, A.; Gola, A.; Cazzanelli, M.; Pavesi, L.; Zorzi, N.; Piemonte, C. Characterization of Single-Photon Time Resolution: From Single SPAD to Silicon Photomultiplier. *IEEE Trans. Nucl. Sci.* **2014**, *61*, 2678–2686. [CrossRef]
20. Acerbi, F.; Paternoster, G.; Gola, A.; Zorzi, N.; Piemonte, C. Silicon photomultipliers and single-photon avalanche diodes with enhanced NIR detection efficiency at FBK. *Nucl. Instrum. Methods Phys. Res. Sect. A* **2018**, *912*, 309–314. [CrossRef]
21. Wavelength Electronics. WHY5640 Temperature Controller. Available online: https://www.teamwavelength.com/product/why5640-2-2-a-temperature-controller/ (accessed on 16 April 2021).
22. Behera, A.; Di Sieno, L.; Pifferi, A.; Martelli, F.; Mora, A.D. Instrumental, optical and geometrical parameters affecting time-gated diffuse optical measurements: A systematic study. *Biomed. Opt. Express* **2018**, *9*, 5524–5542. [CrossRef]
23. Zappalá, G.; Acerbi, F.; Ferri, A.; Gola, A.; Paternoster, G.; Zorzi, N.; Piemonte, C. Set-up and methods for SiPM Photo-Detection Efficiency measurements. *J. Instrum.* **2016**, *11*, P08014. [CrossRef]
24. Ghioni, M.; Gulinatti, A.; Rech, I.; Zappa, F.; Cova, S. Progress in Silicon Single-Photon Avalanche Diodes. *IEEE J. Sel. Top. Quantum Electron.* **2007**, *13*, 852–862. [CrossRef]
25. Wabnitz, H.; Taubert, D.R.; Mazurenka, M.; Steinkellner, O.; Jelzow, A.; Macdonald, R.; Milej, D.; Sawosz, P.; Kacprzak, M.; Liebert, A.; et al. Performance assessment of time-domain optical brain imagers, part 1: Basic instrumental performance protocol. *J. Biomed. Opt.* **2014**, *19*, 86010. [CrossRef]
26. O'Connor, D. *Time-Correlated Single Photon Counting*; Academic Press: Cambridge, MA, USA, 2012.
27. Lange, F.; Dunne, L.; Hale, L.; Tachtsidis, I. MAESTROS: A Multiwavelength Time-Domain NIRS System to Monitor Changes in Oxygenation and Oxidation State of Cytochrome-C-Oxidase. *IEEE J. Sel. Top. Quantum Electron.* **2018**, *25*, 7100312. [CrossRef]
28. Re, R.; Contini, D.; Turola, M.; Spinelli, L.C.; Zucchelli, L.; Caffini, M.; Cubeddu, R.; Torricelli, A. Multi-channel medical device for time domain functional near infrared spectroscopy based on wavelength space multiplexing. *Biomed. Opt. Express* **2013**, *4*, 2231–2246. [CrossRef] [PubMed]